mathematics

MDPI

Article

Graph Theoretic Analyses of Tessellations of Five Aperiodic Polykite Unitiles

John R. Jungck [1,*] and Purba Biswas [2]

[1] Departments of Biological Sciences and Mathematical Sciences, University of Delaware, Newark, DE 19716, USA
[2] Department of Mathematics, Applied Mathematics and Statistics, Case Western Reserve University, Cleveland, OH 44106, USA; purba.biswas@case.edu
* Correspondence: jungck@udel.edu

Abstract

Aperiodic tessellations of polykite unitiles, such as hats and turtles, and the recently introduced hares, red squirrels, and gray squirrels, have attracted significant interest due to their structural and combinatorial properties. Our primary objective here is to learn how we could build a self-assembling polyhedron that would have an aperiodic tessellation of its surface using only a single type of polykite unitile. Such a structure would be analogous to some viral capsids that have been reported to have a quasicrystal configuration of capsomeres. We report on our use of a graph–theoretic approach to examine the adjacency and symmetry constraints of these unitiles in tessellations because by using graph theory rather than the usual geometric description of polykite unitiles, we are able (1) to identify which particular vertices and/or edges join one another in aperiodic tessellations; (2) to take advantage of being scale invariant; and (3) to use the deformability of shapes in moving from the plane to the sphere. We systematically classify their connectivity patterns and structural characteristics by utilizing Hamiltonian cycles of vertex degrees along the perimeters of the unitiles. In addition, we applied Blumeyer's 2×2 classification framework to investigate the influence of chirality and periodicity, while Heesch numbers of corona structures provide further insights into tiling patterns. Furthermore, we analyzed the distribution of polykite unitiles with Voronoi tessellations and their Delaunay triangulations. The results of this study contribute to a better understanding of self-assembling structures with potential applications in biomimetic materials, nanotechnology, and synthetic biology.

Keywords: aperiodic tessellations; graph theory; Hamiltonian cycles; polykites; chirality; periodicity; Heesch number; corona; surround number; Voronoi tessellations; Delaunay triangulations; Pitteway violations

MSC: 05c90

check for updates

Academic Editor: Darren Narayan

Received: 30 July 2025
Revised: 6 September 2025
Accepted: 12 September 2025
Published: 15 September 2025

Citation: Jungck, J.R.; Biswas, P. Graph Theoretic Analyses of Tessellations of Five Aperiodic Polykite Unitiles. *Mathematics* **2025**, *13*, 2982. https://doi.org/10.3390/math13182982

Copyright: © 2025 by the authors. Licensee MDPI, Basel, Switzerland. This article is an open access article distributed under the terms and conditions of the Creative Commons Attribution (CC BY) license (https://creativecommons.org/licenses/by/4.0/).

1. Introduction

The excitement regarding unitiles composed of polykites (Smith et al., 2023a,b) [1,2] that are capable of aperiodic tessellations has been enormous. To date, most of the literature has described five such unitiles composed of polykites, hats, turtles, hares, red squirrels, and gray squirrels, in terms of their geometry. Because we (Jungck et al., 2023) [3] as well as others (Twarock, 2004, 2006; Todd, 2018) [4–6]; Konevtsova, Lorman, and Rochal, 2015 [7]) are concerned with modeling the self-assembly of viral capsids with three dimensional aperiodic tessellations of unitiles on polyhedra, we need to morph 2D tiles to curvilinear

3D tiles. We build self-assembling mesomodels of viral capsids via 4D printing in order to generate "virosomes," which are nanocapsules that can act as carriers of drugs in medical applications. In (Jungck et al., 2025) [8], we enumerated six important benefits of such drug delivery vehicles: "(1) Higher dose loading with smaller dose volumes; (2) Longer site-specific retention; (3) More rapid absorption of active drug substances; (4) Increased bioavailability of the drug; (5) Higher safety and efficacy; (6) Improved patient compliance. Furthermore, nanocapsules made of viral capsids ("virosomes") have the additional advantages of being biodegradable, biocompatible, and non-toxic as well as being able to incorporate surface antigens appropriate for particular target issues."

In our prior work on self-assembly and self-folding of dodecahedra and icosahedra, we were able to use Dodd, Damasceno, and Glotzer's (2018) theorem [9] for classifying all 86,760 different Dürer nets by using a Hamiltonian cycle of degrees of vertices on the perimeter of each Dürer net. Herein, we have used the same graph theoretic assignment of a Hamiltonian cycle of degrees of vertices on the perimeter of each polykite for hats, turtles, hares, and red and gray squirrels (Figure 1 and Table 1). In tessellations, identification of which vertices or edges bind to one another is specified uniquely by the series of consecutive vertices or edges. Our eventual goal is to physically produce self-assembling polyhedra composed of an aperiodic homochiral tessellation of unitiles. Furthermore, because viral capsids are self-assembled, we are interested in developing "matching rules" (Kaplan, 2021 [10]) for which edges and vertices of unitiles are in contact with one another in a tessellation. As the sum of angles of triangles is very different on planes and spheres, we prefer to classify the polykites in graph theoretic terms in terms of the degrees of vertices on the outer perimeter of polykites.

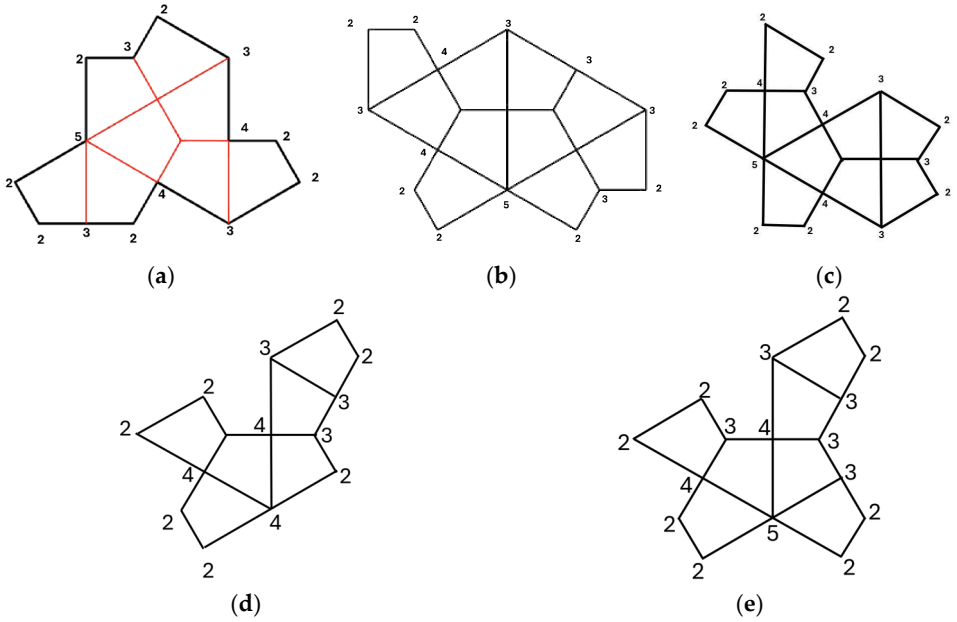


Figure 1. (**a**) Hat, (**b**) turtle, (**c**) hare, (**d**) red squirrel, and (**e**) gray squirrel as polykites with Hamiltonian cycle of degrees of vertices. We include the edges of the polykites, but we do not include vertices on the interior of the polykites. The Hamiltonian cycle of degrees of vertices connects every vertex of the respective polykite.

Table 1. Hamiltonian cycle of degrees of vertices for hats, turtles, red squirrels, hares, and gray squirrels.

Vertex Number	**1**	**2**	**3**	**4**	**5**	**6**	**7**	**8**	**9**	**10**	**11**	**12**	**13**	**14**	**15**	**16**
	Vertex degree in Hamiltonian cycle															
Hat	2	3	2	3	4	2	2	3	4	2	3	2	2	5		
Turtle	2	2	4	3	3	3	2	3	2	5	2	2	4	3		
Red Squirrel	2	2	3	4	3	2	2	3	3	2	4	2	2	4		
Hare	2	2	4	2	2	3	4	3	2	3	2	3	4	2	2	5
Gray Squirrel	2	2	3	4	3	2	2	3	3	3	2	2	5	2	2	4

In Section 2, we use these Hamiltonian cycles of degrees of vertices to describe junctions between adjacent polykites in tessellations and lay the foundation for developing rules for tessellations. In Section 3, our third perspective is derived from teaching a course entitled Ethnomathematics: Art, Culture, and Social Justice. We believe that the graph theory approach is easily accessible to students and helps students appreciate the historical importance of contributions of artisans from around the globe in their production of artistic tessellations. In Section 4, we examine tessellations from the perspective of Heesch numbers for the coronas of tiles around an initial tile. Finally, in Section 5, we extensively use graph theory to analyze biological tessellations with our software package Ka-me (version 1.0): A Voronoi Image Analyzer (Khiripet, Khantuwan, and Jungck, 2012) [11]; Jungck et al., 2021) [12]. One particular tool in our package that is helpful in analyzing aperiodic tessellations is the Delaunay triangulation, which helps us compile which configurations are nearest neighbors.

We have demonstrated that graph theory analysis of aperiodic tessellations provides a powerful alternative to current geometric descriptions because it allows us to classify adjacency patterns and structural characteristics using Hamiltonian cycles of vertex degrees. These Hamiltonian cycles can be used to identify vertex and edge interactions uniquely. Each polykite unitile (hat, turtle, hare, red squirrel, gray squirrel) was uniquely characterized by a Hamiltonian cycle of vertex degrees along its perimeter. This allowed for precise identification of vertices and edges, thus clarifying adjacency and binding rules essential for self-assembly processes, which are especially relevant in biological contexts like viral capsid formation.

2. Hamiltonian Cycles

An advantage of identifying polykites by the Hamiltonian path of degrees of the vertices on their perimeters is that it allows us to determine the address of each vertex and edge, as we want to know which edges and vertices interact with one another at different frequencies in various tessellations. In Table 1, we identify the Hamiltonian cycle of degrees of vertices for Smith's five polykites.

As shown in Table 1, on the one hand, the Hamiltonian cycle does visit every vertex on the perimeter once and only once. On the other hand, the Hamiltonian cycle described herein does not satisfy either Dirac's Theorem (Li, 2013 [13,14]) (if every vertex has a degree of at least n/2) or Ore's Theorem (1960, [15] (if the sum of degrees of any two non-adjacent vertices is at least n), but the criterion that each vertex is included once and only once in a series of contiguous vertices is satisfied. No permutation of any cycle of equal lengths of two different polykites can produce identical sequences. For example, hat's sequence with a 5 in it (22,523) is not identical to turtle's sequence with a 5 in it (32,522), and a red squirrel has no degree 5 vertex at all.

By using the center vertex of a five-vertex string, we can uniquely identify a vertex. For example, vertex 3 of a turtle has the address 22,433, which does not occur for any other

vertex in this or any of the other polykites. Similarly, an edge between two vertices can be identified as the edge between the second and third vertex degrees in a four-vertex address. As above, the edge between vertices 8 and 9 of a turtle has the address 2325.

Furthermore, we observed ten distinct orientation types of local vertex configurations on tessellations of specters (Table 2), primarily involving X-, Y-, and T-type junctions, as they appear in specter tilings. These junctions refer to the ways in which tiles meet at vertices. X-junctions involve four specters converging at right angles; Y-junctions feature three tiles meeting at 120° angles; and T-junctions occur when one tile's edge terminates against the side of another. The spatial distribution and frequency of these junctions reveal key structural constraints in specter tilings. In the context of viral capsids, we were motivated by Esque, Oguey, and de Brevern (2011) [16], who determined protein contacts in Voronoi tessellations.

Table 2. Vertex configurations in tessellations of spectre unitiles.

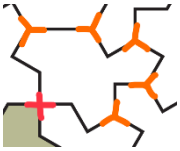
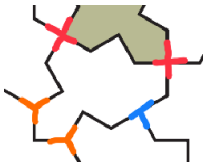
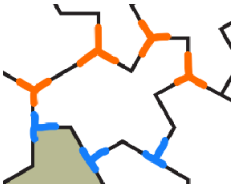
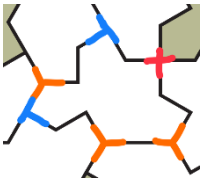
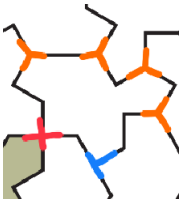
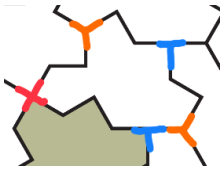
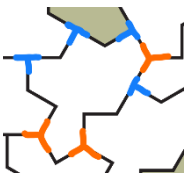
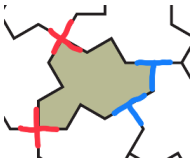
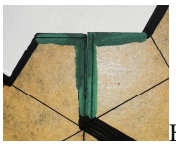
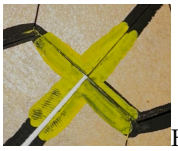
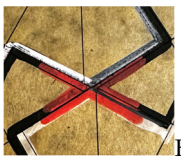
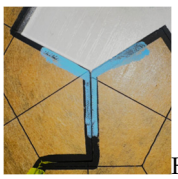
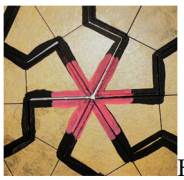
Images	Junctions	Images	Junctions
	1X 5Y 0T		0X 5Y 1T
	1X 4Y 0T		2X 2Y 1T
	0X 4Y 3T		1X 3Y 2T
	1X 4Y 1T		1X 2Y 2T
	0X 3Y 4T		2X 0Y 2T

Table 2, in an aperiodic tiling of specters, we identified ten different sub-patterns of adjacency among neighboring tiles. Later in the paper, we will discuss these observations in the context of distinguishing tessellations as periodic versus nonperiodic and homochiral versus heterochiral configurations. In all cases, only a few kinds of junctions identified in Table 2 were represented in different classifications of tessellations of polykites.

In general, analyses of tessellations on hats, turtles, hares, gray squirrels, and red squirrels lend themselves to this type of analysis of surrounding junctions and have different distributions of usage of the nine different kinds of junctions identified in Table 3.

Table 3. Vertex configurations identified among tessellations of the five polykites.

Type	Vertex Degree	Incoming Angles of Unitiles	Unitiles in Tessellation	Images
T	3	90, 90, 180	Hats, Turtles, Hares	 Hare
X Type 1	4	90, 90, 90, 90	Hats, Turtles, Hares	 Hare
X Type 2	4	120, 120, 60, 60	Hats, Turtles, Hares	 Hare
X Type 3	4	120, 60, 120, 60	Hats, Turtles, Hares	 Hare
Y	3	120, 120, 120	Hats, Turtles, Hares	 Hare
H Star Type 1	6	60, 60, 60, 60, 60, 60	Hares	 Hare
P Star Type 2	5	120, 60, 60, 60, 60	Hare	 Hare
I	(0,4)	180, 180	Red Squirrel	 Red Squirrel
R	3	60, 60, 240	Gray Squirrel	 Gray Squirrel

Our classification of junctions of tiles in a tessellation in Table 3 is similar to prior work on Penrose tessellations. Although this prior work showed the configurations, they did not add the details of degrees or vertices or the angles involved in each configuration. The vertex neighborhoods of aperiodic tiles completing a 360° junction (Figure 2) have been reproduced multiple times since Martin Gardner (1977; 1997) [17,18] popularized the discovery of Penrose's pair of tiles (e.g., de Bruijn, 1981 [19]; Doroba and Sokalski, 1991 [20]; Gummelt, 1996 [21]; Flicker, Simon, and Parameswaran, 2020 [22]; Ghose, 2021 [23]) or slight modifications with different names (Yan et al., 2020 [24]). We constructed Table 4 with degrees, angles, and tiles analogous to Table 3.

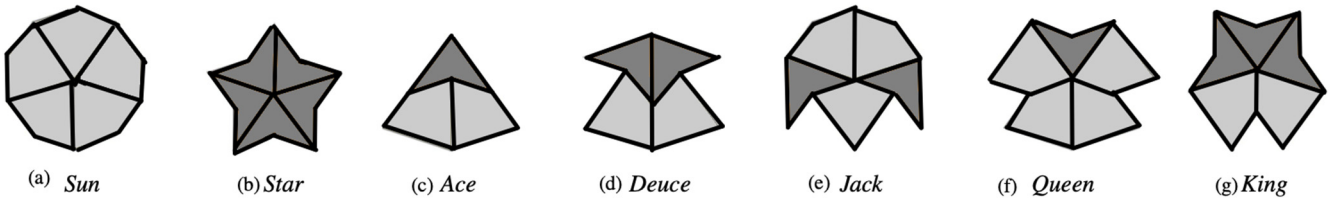


Figure 2. The seven "vertex neighborhoods" of aperiodic tiles completing a 360° junction (modified from WikiCommons Creative Commons license 4.0). Also referred to as "The types of the vertices in the Penrose "kite and dart" lattice.".

Table 4. The degrees of vertices in various named vertex neighborhoods; the angles involved and the tiles involved are enumerated.

Name of Configuration	Degree of Vertex	Angles Involved	Tiles Involved
(a) Sun	5	72, 72, 72, 72, 72	5 Kites
(b) Star	5	72, 72, 72, 72, 72	5 Darts
(c) Ace	3	216, 72, 72	1 Dart, 2 Kites
(d) Deuce	4	36, 36, 144, 144	2 Darts, 2 Kites
(e) Jack	5	36, 72, 72, 36, 144	2 Darts, 3 Kites
(f) Queen	5	72, 72, 72, 72, 72	1 Dart, 4 Kites
(g) King	5	72, 72, 72, 72, 72	3 Darts, 2 Kites

Similarly to Table 3, the identification of degrees of vertices involved in a junction of adjoining tiles and the angles involved in completing a 360 degree closure shown in Table 4 are again sufficient to identify the seven different configurations, Sun, Star, Ace, Deuce, Jack, Queen, and King, of Penrose tiles.

Proposition 1. *For any polykite unitile, there exists a closed traversal of its perimeter that visits each boundary vertex exactly once (i.e., a Hamiltonian cycle through the boundary vertices). This labeled cyclic ordering of the perimeter vertices provides a unique Hamiltonian encoding of the unitile's boundary, which can be used to uniquely match corresponding vertices and edges between unitiles in a tessellation.*

Proof. By the geometric structure of a polykite, its outer boundary forms a single continuous loop. We denote the boundary vertices as nodes and connect adjacent ones along the perimeter, and they form a cyclic graph. Thus, the perimeter itself is a Hamiltonian cycle on the graph of boundary vertices, passing through each vertex exactly once before returning to the start. We obtain a closed labeling traversal by assigning labels to these vertices in sequence around the loop. Such a traversal is guaranteed to exist for any single-piece

polykite because the tile's boundary is a simple closed polygonal chain (each boundary vertex connects to exactly two boundary edges, one on each side). □

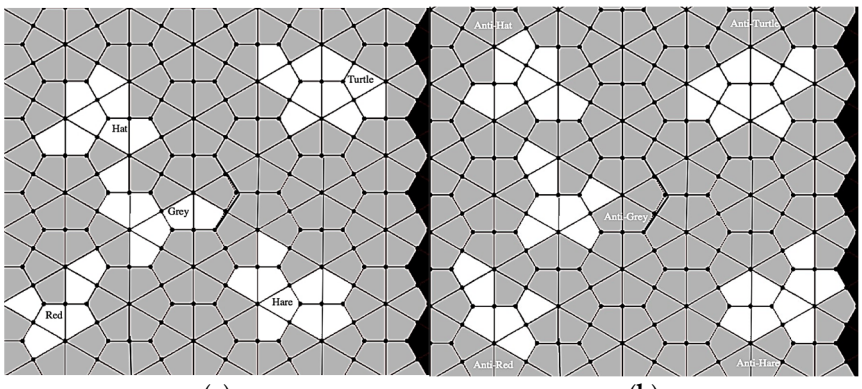
Remark 1. *Classical graph theory provides sufficient conditions for a graph to be Hamiltonian, but these do not directly apply here. Dirac's Theorem (1952) [13,14] and Ore's Theorem (1960) [15] guarantee the existence of a Hamiltonian cycle in an arbitrary graph under certain minimum-degree conditions on the graph's vertices. In our setting, however, the degrees used in the perimeter encoding are not graph–theoretic vertex valencies (number of incident edges); instead, they are vertex classification labels assigned to the tile's boundary vertices.*

In summary, encoding a unitile's perimeter as a Hamiltonian cycle of labeled vertices allows for vertex-addressable identification of every corner and edge of the tile. Each boundary vertex receives a unique address (its position in the cyclic sequence), so one can pinpoint which specific vertices and edges correspond between tiles when multiple unitiles tessellate the plane. This capability forms the basis for the adjacency and chirality analyses in later sections. With a unique perimeter code for each unit, we can systematically track how tiles meet (which vertices/edges coincide) and determine how tile orientations or mirrorings (anti-polykites) contribute to the overall tiling configuration (Table 4).

Our detailed analysis of vertex configurations in Table 4 identified nine distinct types (T, X Type 1, X Type 2, X Type 3, Y, H Star, P Star, I, and R), elucidating how different tiles interacted at their edges and vertices. These junction types revealed essential structural constraints underlying tessellation patterns, indicating how local adjacency rules governed global periodicity or aperiodicity. We intend to explore whether these binding interactions will help us develop a self-assembling aperiodic tessellated polyhedral of unitiles to model quasicrystal-like polyhedral viral capsids, which do not fit the classical Caspar–Klug [25] rules.

3. Ethnomathematics and Education

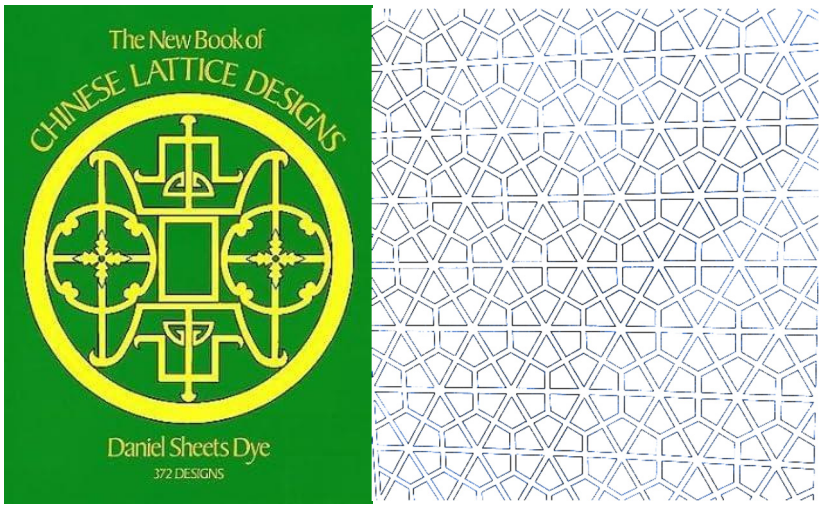
The third perspective we bring to this project derives from teaching a course entitled Ethnomathematics: Art, Culture, and Social Justice. The deltoidal trihexagonal grid graph paper employed to display the polykites and their mirror image (anti-polykites) (Figure 3) goes back to ancient Chinese lattices (Dye, 1981) [10] (Figure 4)



(**a**) (**b**)

Figure 3. Polykites on a deltoidal trihexagonal grid: (**a**) hat, turtle, hare, red squirrel, and gray squirrel. (**b**) Anti-hat, anti-turtle, anti-hare, anti-red squirrel, and anti-gray squirrel.

Thus, as shown in Figure 3, each of the five polykites, hat, turtle, hare, red squirrel, and gray squirrel, consists of 6 to 10 adjacent kites, and each of them is associated with an "anti-polykite," which is equivalent to flipping them over to change to a non-superimposable configuration.



(**a**) (**b**)

Figure 4. (**a**) Book cover of *The New Book of Chinese Lattice Designs* (Dye, 1981) [26]; (**b**) deltoidal trihexagonal grid of a Chinese Lattice. The deltoidal trihexagonal tiling is a dual of the semiregular tiling known as rhombitrihexagonal tiling (Sloane, 2020; [27]). Gene Boggs [28] shares a program for generating deltoidal trihexagonal graph paper that he and others refer to as a "Kitegrid.".

Coulbois et al. (2024) [29] refer to these latices in Figure 4 as "Kitegrids" and note that "The work is very interesting, . . . because two of these tiles (the Hat and the Turtle) are polykites and can be embedded in a Kitegrid, which is the dual of an Archimedean tiling (which can be seen as the Cayley graph of a group), suggesting that the Hat and the Turtle tilings can also be seen as tilings of a group." Previously, Shutov and Maleev (2015) [30,31] called such grids of Penrose tiles the dual of Archimedean tiling and related them to Cayley graphs of groups. Thus, even basic deltoidal trihexagonal tiling is open to exploration through higher mathematics, as well as artistic construction.

An ethnomathematics chapter, "Geometry and Art" by Julian Williams [32], is in a book that picked up on these *Chinese Lattice Designs*, Nelson, Joseph, and Williams' (1993) *Multicultural Mathematics: Teaching Mathematics from a Global Perspective*, which focused particularly on exercises with polykites on this lattice. Williams [32] argued:

> At . . . the second stage of development, children's practical activity with shape and their discussion of their findings develops a conscious knowledge of the properties of shapes. The number of sides, size of angles, and symmetry of figures all become the object of experiment and discovery. Investigating the Chinese lattice design in [Figure 4b] for shapes which tessellate, we find equilateral triangles, hexagons, parallelograms, rhombuses, kites, and trapeziums. . . . Investigating the angles and angle-sums of the various polygons in the design follow very simply from knowing the angles of the kite, i.e., 60°, 90°, 120°, 90°. . . . that area ratios are the squares of length ratios. So, it appears we have an area ratio of 1: $\sqrt{3}$. Indeed, application of trigonometry shows that this is the case, since the lengths of the sides of the kite are in the ratio cos 60°: sin 60°, or ½: $\sqrt{3}/2$ or 1: $\sqrt{3}$. {Pages 148–150}

Williams [32] goes on to engage students in generating and studying symmetry groups of reflections and rotations, as well as using the "Chinese Lattice design as a tessellation of kites, made by taking many kite tiles and fitting them together by trial and error." We can only wonder whether some of the students in Williams' classes may have already built hats, turtles, hares, or red and gray squirrels thirty years ago. Furthermore, we celebrate Williams' inclusion of both art as a "motivating factor of studying a *real* and *attractive*

design" and multicultural appreciation, as we have seen with the current explosion of art based on the discovery of aperiodic tessellations of hats, turtles, and hares.

We believe that classes in ethnomathematics could use our elementary graph theoretic analyses so that students can explore controversies, such as whether other cultures have historically already produced aperiodic tessellations in their art. For example, Ouazene (2023) [33] argues that Moroccan and Andalusian craftspeople generated tiling patterns that are quasicrystalline, while Cromwell (2015) [34] raised skepticisms about previous claims. Ghose (2021) [23] has already reported that engaging students with aperiodic tessellations of Penrose tiles increased young students' confidence, allowed them to compare and contract their aperiodic tessellations and periodic tilings of polygons, and helped them develop an appreciation for "never being able to predict what happens next—the true essence of aperiodic tiling was the clear message received by all." Their mathematical artwork was appreciated by their parents, as well. Kerins et al. (2018) [35] promote the adage "To think deeply about simple things" in their introduction to emphasize the importance of activities involving students in the exploration of nonperiodic tilings of planes, along with the excitement in many communities about the discovery of polykites and aperiodic tessellations. These patterns offer great potential for exploration by students in ethnomathematics courses.

4. Chirality and Periodicity

4.1. Chirality in Tiling

A planar tile T is chiral if it is not congruent with its mirror image, i.e., the tile has a distinct handedness (left vs. right) (Blumeyer, 2023, [36]). In the context of tilings, we call a monohedral tiling homochiral (same handedness) if all copies of the tile share the same orientation (only one enantiomorph is used). Conversely, a heterochiral tiling (different handedness) utilizes a combination of both left- and right-handed versions of the tile. There is no middle ground; if even a single tile is the opposite handedness of another, the tiling is heterochiral. In practical terms, homochiral tilings use only rotations and translations (orientation-preserving isometries), whereas heterochiral tilings also include reflections (orientation-reversing isometries that flip handedness) (Blumeyer, 2023, [36]).

4.2. Periodicity in Tiling

A tiling is periodic if it repeats under translations in two independent directions. Formally, there exist vectors $t_1, t_2 \in R^2$ such that the entire pattern is invariant under translation by any linear combination of t_1, t_2. The fundamental domain is the minimal region of the tiling that generates the whole pattern through such translations (Grünbaum & Shephard, 1987 [37]).

A tiling is nonperiodic if no such translational symmetries exist. A tile is called aperiodic if every tiling it admits is nonperiodic (Blumeyer, 2023 [36]). In other words, no arrangement of copies of an aperiodic monotile can yield a periodic tiling. This contrasts with common prototiles, such as squares or hexagons, which easily admit periodic tilings. Importantly, nonperiodicity can often be enforced by purely local matching rules, as first formalized in the context of quasiperiodic tilings by Le (1997) [38].

Unless otherwise stated, the term aperiodic assumes the full symmetry group of the Euclidean plane, including reflections. Thus, if a tile avoids periodicity only when reflections are forbidden, it is classified as a special case of aperiodicity.

4.3. Blumeyer's 2 × 2 Classification Framework

Using the concepts of periodicity and chirality, monotile (unitile) tessellations can be classified as periodic vs. nonperiodic and homochiral vs. heterochiral. Douglas Blumeyer

(2023) [36] proposed a clear and insightful 2 × 2 framework that captures these distinctions and organizes known aperiodic monotiles accordingly. This classification highlights structural differences in how a tile can (or cannot) tile the plane, depending on whether reflections are allowed and whether translational symmetry is present. This yields four quadrants.

4.3.1. Periodic Homochiral (PH)

Periodic homochiral (PH) tiling repeats periodically and is homochiral as it uses only one tile handedness. The tile can form a regular repeating pattern without needing its mirror.

4.3.2. Periodic Heterochiral (PHetr)

Periodic Heterochiral (PHetr) tiling (Voigt et al., 2025) [39] is periodic overall, but it requires a mixture of both orientations of the tile to achieve a repeating pattern. In this case, the tile can tile periodically, but not if restricted to one-handed copies; the periodic pattern intrinsically uses pairs of mirrored tiles.

4.3.3. Nonperiodic Homochiral (NH)

Nonperiodic homochiral (NH) tiling is a forced nonperiodic (aperiodic) tessellation, but it achieves this using tiles of only one chirality. In other words, the tile does admit tilings with no translational symmetry, yet we never need to use the mirror form—all tiles can be oriented identically (a chiral tiling, Blumeyer (2023) [36]).

4.3.4. Nonperiodic Heterochiral (NHetr)

Nonperiodic Heterochiral (NHetr) tiling is aperiodic (no global periodic order), 3.3.4 and, moreover, any tiling of this tile must be heterochiral. This is the category of the original Einstein monotile discovery: the hat tile (and its mirror-symmetric partner and the turtle) are aperiodic monotiles that inherently mix handedness. These tiles thus belong to the nonperiodic heterochiral class; they admit only nonperiodic tilings, and those tilings are inevitably two-handed.

Figure 5 illustrates this classification framework; Blumeyer's survey provided examples in three quadrants (PHetr, NH, NHetr), but the periodic homochiral (PH) quadrant was left blank.

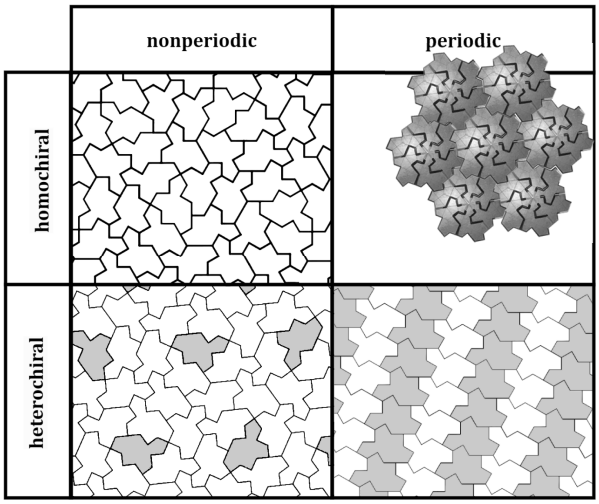


Figure 5. Blumeyer's (2023) [13] 2 × 2 framework (revised with permission from Blumeyer). We have added the homochiral, periodic example of polykite supertiles of hares.

4.4. Filling the Missing Quadrant: The Hare

Proposition 2. *The hare polykite admits periodic homochiral tiling, providing the first explicit example in Blumeyer's PH category.*

Proof. We construct a supertile of six hares arranged symmetrically around a central junction. This supertile satisfies three structural constraints. (i) Edge pairing: The boundary edges of the six-hare supertile form parallel, oppositely oriented pairs, ensuring closure under translation. (ii) Junction consistency: The internal junctions propagate consistently across the plane and contain no anti-hares. (iii) Rotational symmetry: The supertile has at least two-fold rotational symmetry, giving two independent translation vectors. By repeating this supertile across the plane, we obtain a tiling that is simultaneously periodic and homochiral. No anti-hares are required at any stage. Thus the hare fills the previously empty PH quadrant. □

Proposition 3. *With the hare providing a PH example, all four categories of Blumeyer's framework [35] are now represented by known polykite or monotile tessellations.*

Proof. Blumeyer's original classification left PH blank. Proposition 3 demonstrates constructive PH tiling by hares, completing the framework, as shown in Figure 5. □

4.5. Other Polykites

Hat and turtle are both proven aperiodic monotiles [1,2]. Any attempt at homochiral periodic construction fails because of orientation–parity mismatches in their edge vectors. Thus, they belong to the nonperiodic heterochiral (NHetr) and NH class. The specter tile (Tile(1,1)) allows for periodic tilings, but only heterochiral ones. Its boundary constraints block periodic homochiral closure, confirming its role in the NH, PHetr, and NHetr categories. For red and gray squirrels, we observed that both admit periodic tilings, but only in heterochiral configurations. Whether homochiral supertiles exist remains an open problem.

In Table 5, we summarize our analysis of tessellations of the five polykites. Although these results extend Blumeyer's framework, they remain preliminary. Important open directions include testing the unexplored possibility of aperiodicity in the hare, accurately enumerating polykite configurations, and carrying out a deeper analysis of chirality and Blumeyer classifications. A key question is whether other polykites (such as the squirrel tiles) can also admit homochiral periodic assemblies, or whether the hare is unique in this regard. Future work will investigate larger supertile constructions and the conditions under which aperiodicity may emerge in the hare to address these questions.

Therefore, we believe that we have demonstrated the utility of employing Blumeyer's (2023) [36] framework to investigate chirality and periodicity within tessellations. By employing Blumeyer's classification framework, we categorized unitiles along axes of periodicity (periodic vs. nonperiodic) and chirality (homochiral vs. heterochiral). Notably, this research introduces a previously unrepresented configuration: periodic homochiral tessellation via the hare tile. The classification effectively captures structural distinctions, significantly advancing our understanding of tile interaction possibilities and constraints.

Table 5. Classification of polykite unitiles (chirality vs. periodicity).

Tile (Unitile)	Number of Polykites	Periodicity	Chirality		Class (Blumeyer 2×2)
			Homochiral	Heterochiral	
Hat	8	Nonperiodic/Periodic	N	Y	NH, NHetr
Turtle	10	Nonperiodic	N	Y	NH, NHetr
Hare	9	Periodic	Y	Y	PH, PHetr
Gray Squirrel	6	Periodic	Y	N	PHetr
Red Squirrel	7	Periodic	Y	N	PHetr
Spectre	N/A	Periodic and Nonperiodic	Y	Y	NHetr, NH, PHetr

5. Corona Structures and Heesch Numbers in Polykite Tilings

In tiling theory, a tile corona (or k-corona) of a given tile is defined as the local neighborhood consisting of k concentric layers of adjacent tiles surrounding it (Adams, 2022) [40]. Formally, the 0th corona of a tile T is just T itself, and for $k > 0$, the kth corona includes all tiles sharing an edge with the $(k-1)$th corona. To completely form its first corona around the central tile, the minimum number of congruent copies of a tile needed is defined as the surround number ((Adams, 2022) [40]; and (Friedman, n.d.) [41]). Each corona layer effectively represents one ring of tiles around a central seed tile, reflecting local adjacency constraints and neighbor relationships.

Using coronas, the Heesch number of a shape can be defined ((Adams, 2022) [15]; and (Mann, 2004) [42]; and Weisstein, n.d. [43]). The Heesch number is the maximum number of complete corona layers of congruent copies of a shape that can surround it without gaps or overlaps. Thus, a shape with Heesch number k can form exactly k rings of identical tiles around it but fails at the $(k+1)$th layer. For example, squares, equilateral triangles, and hexagons tile the plane regularly, giving it an infinite Heesch number (∞), while a circle cannot form a complete corona even once, thus having Heesch number 0. Generally, shapes that tile the plane have infinite Heesch numbers, implying no finite limitation on forming successive coronas. The number of tiles that is included in the first corona is called the surround number. In Figure 6, the coronas for hares and anti-hares are shown.

Beyond the standard Heesch number, a related concept is the quasi-Heesch number, which relaxes the requirement that the central region matches the surrounding tile. Instead, a different shape or "hole" is placed at the core, and layers of a single tile type are built around it until no further growth is possible (Locke Demosthenes, 2023) [44].

For instance, the "hat" monotile has a demonstrated quasi-Heesch number of eight, able to surround a hexagonal gap completely through eight layers before failing (Kaplan, 2021) [45]. The surround number of the first corona is six. The tile counts per corona layer are shown in Figure 7. The monotonically increasing pattern always adds some multiple of six. In Table 6, we call out this pattern.

Corona layers increase approximately by multiples of six initially (surround number six), but growth becomes irregular after the fifth layer. After the eighth layer, attempts to continue fail due to breakdowns in geometric compatibility and growing asymmetries, i.e., a full ninth corona cannot be completed without violating local tiling rules or creating gaps. This behavior justifies a quasi-Heesch number of eight for the hat tile (Locke Demosthenes, 2023) [44].

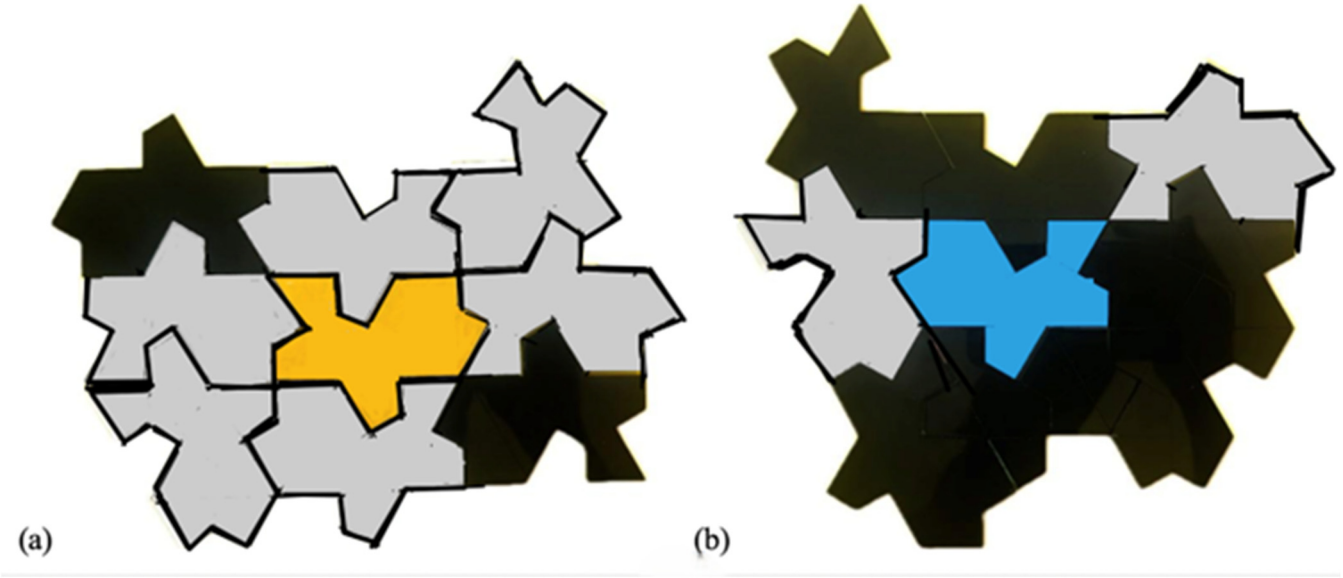


Figure 6. (**a**) Hare and (**b**) anti-hare coronas are shown. The surround number is eight in each case, as they are simply flipped versions of one another. Thus, the corona of a hare unitile has six anti-hares and two hares in the corona (**a**), and the anti-hare has six hares and two anti-hares in its corona (**b**). We believe that both have a Heesch number of one, as we have not successfully tiled another corona.

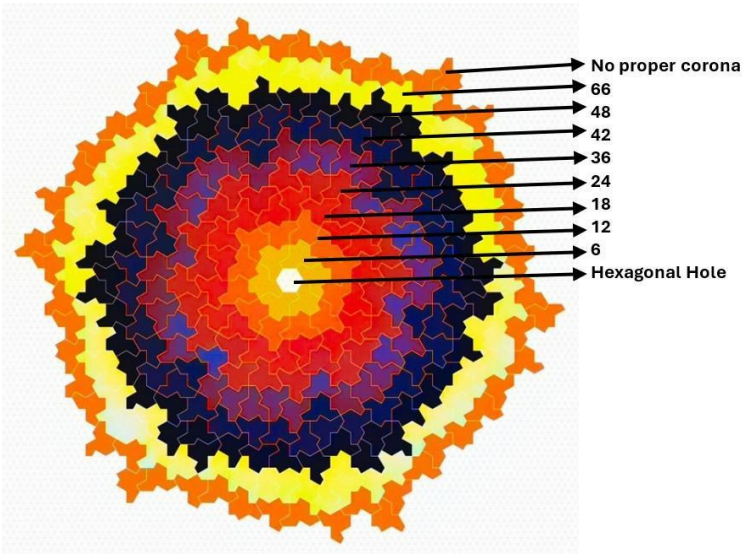


Figure 7. Corona layers of hat tile (modified from Kaplan, 2021) [20].

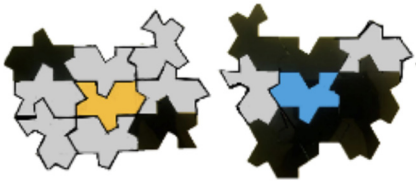
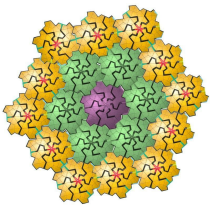
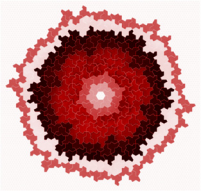
Table 6. Corona layers of hat tile.

Corona Layer (k)	**1**	**2**	**3**	**4**	**5**	**6**	**7**	**8**	**N\A**
Tile Count	6 (surround number)	12	18	24	36	42	48	66	N\A

The concepts of coronas and Heesch numbers have been extensively studied by Adams (2022) [40], Mann (2004) [42] and (Kaplan, 2021) [45], particularly in contexts where finite corona layers provide insights into local tiling feasibility or demonstrate non-tiling behaviors. They contrast notably with shapes that have finite Heesch numbers, such as Mann's previously studied "5-hexapillar" tile, which achieved a Heesch number of five without fully tiling the plane (Mann (2004) [42]).

Even though not all tiles in the polykite family, such as the hat, turtle, hare, red squirrel, and gray squirrel, share the same global tiling behavior, their local tiling characteristics can still be systematically analyzed using surround numbers, Heesch numbers, and corona layer growth. To better understand the local complexity and structural properties of hat and hare monotiles, we propose a detailed comparative table shown in Table 7 to evaluate some other corona patterns in polykite tessellations.

Table 7. Corona layers of tile.

Heesch Number	Corona Layer	Surround Number	Quasi-Heesch Number	Tile Name	Image
H = 1	1	8	N\A	Hare	(a) 
H = ∞	∞	6	N\A	Hare	 (b)
H = 8	8	6	8	Hat	 (c)

Note that in 7 (b) the starting tile is a supertile of six hares and that each tile in the corona is also a supertile of six hares.

Analyzing local tiling characteristics using corona structures, their Heesch numbers, and surround numbers and examination of corona structures offered critical insights into local tiling capabilities. For instance, the hat tile displayed a quasi-Heesch number of eight, successfully surrounding a hexagonal hole through eight layers before failing to tile further. Through comparative analyses, we can see variations in corona growth patterns and Heesch numbers among the unitiles, emphasizing the rich diversity of local and global tiling behaviors. The frequency and distribution of these junctions illuminate the structural constraints intrinsic to each tessellation. A detailed exploration of corona structures revealed both finite and infinite Heesch numbers. Comparative analysis of hat, hare, turtle, red, and gray squirrel tiles can demonstrate variations in corona growth and Heesch numbers.

From the perspective of self-assembly models, Heesch numbers describe the local growth potential of a unitile; a finite Heesch number mirrors how protein subunits can only assemble a limited number of layers before geometric incompatibilities halt further growth, while an infinite Heesch number corresponds to assemblies that can propagate indefinitely, like periodic lattices (Adams, 2022 [40]; Mann, 2004 [42]). In contrast, viral capsids must terminate as closed polyhedral shells rather than infinite sheets (Twarock, 2004 [4]; Konevtsova, Lorman, and Rochal, 2015 [7]). Thus, combining Hamiltonian cycle encodings (for precise boundary matching rules) with Heesch and corona analysis (for local

growth feasibility) provides a graph–theoretic analogue of how self-assembling capsomers form finite, quasicrystalline capsids (Jungck et al., 2023 [3]; Jungck et al., 2025 [8]). Moreover, when interpreted through Blumeyer's chirality–periodicity framework, Heesch numbers highlight why certain polykites (e.g., specters, hats, and turtles) enforce nonperiodicity while others (e.g., hares) enable periodic homochiral growth, underscoring how local growth constraints and global symmetry classes jointly govern self-assembly outcomes (Blumeyer, 2023 [36]; Voigt et al., 2025 [39]).

6. Voronoi Diagram Analysis with the Ka-me Tool for Aperiodic Tessellations

If we use the centroid of each anti-hat in an aperiodic tessellation composed mostly of hats to serve as generator points for a Voronoi tessellation (Jungck et al., (2021) [12]; Khiripet, Khantuwan, and Jungck, 2012) [11], we observe an amazingly regular pattern, which seems counterintuitive given our expectation for an aperiodic tessellation (Phillips, 2014) [46]. To use Ka-me, users upload an image and then enter each Voronoi generator point on each respective polygon. The software can then automatically generate a matching Voronoi tessellation and produce a histogram of the number of edges per Voronoi cell for those within a convex hull (incomplete polygons on the periphery are thus excluded). A Delaunay triangulation of the Voronoi tessellation and a variety of other geometric and graph theoretic constructions can be turned on. Namely, in Figure 8, we observe that nearly all of the Voronoi cells in the tessellation are hexagons. Furthermore, when we construct the graph theoretic dual, namely a Delaunay triangulation for identifying nearest-neighbors, if we ignore Pitteway violations attached to the convex hull as potentially being artifacts due to incomplete Voronoi cells, then we still find two Pitteway violations (Figure 9).

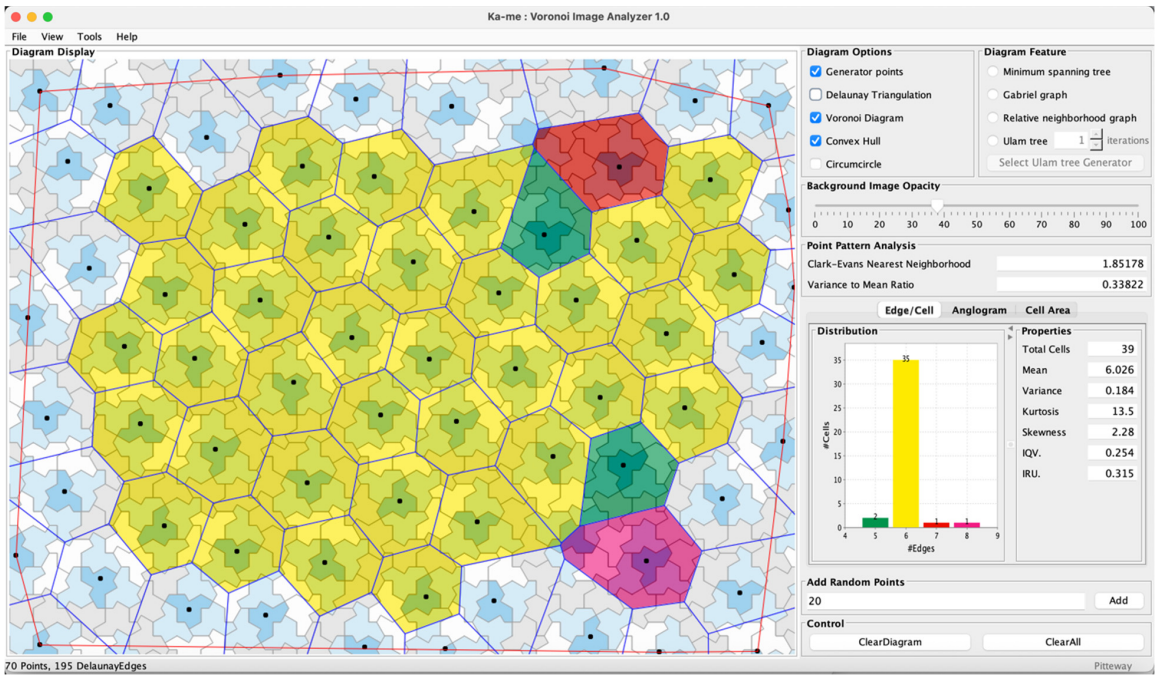


Figure 8. A Ka-me (Khiripet, Khantuwan, and Jungck, 2012) [11] analysis of an aperiodic tessellation of hat monotiles developed by A. P. Goucher [47]. The Voronoi cells that are complete (namely, those within the convex hull) are colored by their number of sides. The histogram at the right demonstrates the distribution of 5-, 6-, 7-, and 8-sided Voronoi cells. The centroid of each anti-hat is created using a generator point of respective Voronoi cells in a tessellation of the plane. At the bottom left, the 70 anti-hats are the number of Voronoi generator points. However, only 39 are inside of the convex hull. Despite the aperiodicity in the tessellation, note that only 4 out of 39 Voronoi cells are not hexagons.

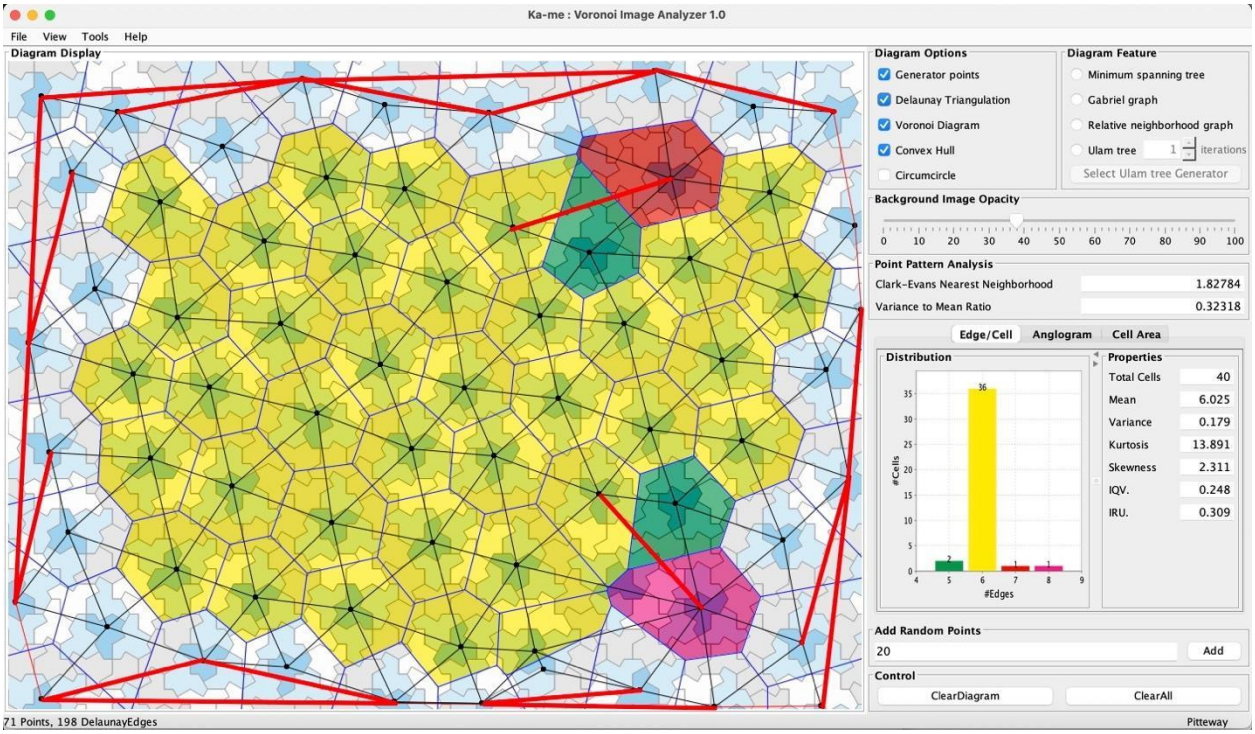


Figure 9. However, the topological dual, the Delaunay triangulation of the Voronoi tessellation, is irregular, which again illustrates that the graph theoretical analysis of an aperiodic tessellation identifies patterns. The number of Delaunay edges is 198 (shown at the lower left). In particular, we draw your attention to Pitteway violations (red lines; the word Pitteway is highlighted at the lower right screen and bolded if violations occur), i.e., Pitteway violations are Delaunay edges that transverse more than one Voronoi edge. So, while the Voronoi tessellation is principally composed of hexagonal cells, there are numerous Pitteway violations on the Delaunay triangulation. While many Pitteway violations that are on the convex hull of the Voronoi tessellation might be ignored as artifacts of the aperiodic tessellation not extending to infinity, there are two exceptions highlighted in the interior, which are not attached to the convex hull.

Gilevich et al. (2024) [48] have extended our use (Jungck et al., 2021; [12]) of image analysis of Delaunay triangulations of the Voronoi tessellations by adding two colorings. They color a Delaunay edge green if the two Voronoi generator points correspond to Voronoi cells with the same number of sides and red if they have a different number of sides. They prove that such colorings are complete, bi-colored, and semitransitive with a Ramsay number R_{trans} (3,3) = 5. In Figure 9, the red lines would be connected to the four Voronoi polygons with fewer or more than six sides. We have not illustrated these, as we do not believe that this coloring adds anything to our current analysis, but we do believe that coloring of graphs is another useful tool that may be helpful in applying graph theory to aperiodic tessellations.

We hope that the unanticipated regularity in the distribution of anti-hats in an aperiodic tessellation of hats and anti-hats that we discovered by using Voronoi tessellations, Delaunay triangulations, and Pitteway violations will be helpful in further analyses of tessellations of all five polykites.

7. Conclusions

This study's insights have potential applications in biomimetic materials, nanotechnology, synthetic biology, and ethnomathematics. The detailed classification methods contribute significantly to understanding self-assembling structures. Fundamentally, we

re-assert that graph theory has tremendous potential to inform future research on aperiodic tessellations of unitiles.

As a future use of graph theory, we want to explore the construction of Schlegel diagrams in order to guide our 4D printing research. Schlegel diagrams are the topological duals of Dürer nets and would apply analogously to our polykites, as well. Jon-Paul Wheatley has 3D printed a polyhedron, which he calls "The Hat Trick," which has 60 hats and 12 decagons (he calls them pentagons; however, each edge of a pentagon has two adjoining edges of hat tiles) for a tidal of 72 faces [49]. Even if we were comfortable with the 12 hexagonal holes (as the proteins in some viral capsids do not completely enclose the surface of some viral capsids), we would need to produce a Schlegel diagram (Jungck et al., 2023 [3]) to produce a planar projection of which tiles were adjacent to each other and where we would place magnets with oriented north and south poles to successfully produce a self-assembling polyhedron.

Another area that we want to explore is what Akpanya et al. (2024) [50] refer to as kinematic constraints on topological interlocking assembly. They have successfully constructed assemblies of specter monotiles into large planar tessellations. While they have explored the combinatoric and geometric properties of their tessellations, they have not used graph theory.

Author Contributions: Conceptualization, J.R.J.; methodology, J.R.J. and P.B.; validation, J.R.J. and P.B.; formal analysis, J.R.J.; investigation, J.R.J. and P.B.; writing—original draft preparation, J.R.J. and P.B.; writing—review and editing, J.R.J. and P.B.; visualization, J.R.J. and P.B.; supervision, J.R.J.; project administration, J.R.J.; funding acquisition, J.R.J. All authors have read and agreed to the published version of the manuscript.

Funding: This work was supported by the University of Delaware's GEMS Program (Graduate Education in the Mathematical Sciences) of the Department of Mathematical Sciences, the Summer Undergraduate Research Program (SURP), the Delaware INBRE Summer Scholars Program funded by the National Institutes of Health—NIGMS (P20 GM103446), a Sigma Xi (National Scientific Honor Society) outreach grant, and a Society for Mathematical Biology education grant.

Data Availability Statement: The original contributions presented in this study are included in the article. Further inquiries can be directed to the corresponding author.

Acknowledgments: The authors gratefully acknowledge summer undergraduate research students who have built laser cut and three dimensional printed physical models of hats, turtles, hares, red squirrels, and gray squirrels: Joseph Yarbrough, Metehan Cebeci, Ibukun Fagbohun, Leara Cellitti, Mahogony Collins, and Papa Boateng. Colorful artwork on tessellations was done by Skylar Jungck. These physical models were invaluable in examining multiple properties of each of these configurations.

Conflicts of Interest: The authors declare no conflicts of interest.

References

1. Smith, D.; Myers, J.S.; Kaplan, C.S.; Goodman-Strauss, C. An Aperiodic Monotile. *Comb. Theory* **2024**, *4*, 9. [CrossRef]
2. Smith, D.; Myers, J.S.; Kaplan, C.S.; Goodman-Strauss, C. A Chiral Aperiodic Monotile. *Comb. Theory* **2024**, *4*, 2. [CrossRef]
3. Jungck, J.R.; Brittain, S.; Plante, D.; Flynn, J. Self-Assembly, Self-Folding, and Origami: Comparative Design Principles. *Biomimetics* **2023**, *8*, 12. [CrossRef]
4. Twarock, R. A Tiling Approach to Virus Capsid Assembly Explaining a Novel Role for Hexamers. *J. Theor. Biol.* **2004**, *226*, 477–482. [CrossRef] [PubMed]
5. Twarock, R. The Architecture of Viral Capsids Based on Tiling Theory. *J. Theor. Med.* **2005**, *6*, 87–90. [CrossRef]
6. Todd, H. A Class of Spherical Penrose-Like Tilings with Connections to Virus Protein Patterns and Modular Sculpture. In Proceedings of the Bridges 2018: Mathematics, Art, Music, Architecture, Education, Culture, Stockholm, Sweden, 25–29 July 2018; Tessellations Publishing: Phoenix, AZ, USA, 2018; pp. 237–244.

7. Konevtsova, O.G.V.; Lorman, V.L.; Rochal, S.B. Structures of Spherical Viral Capsids as Quasicrystalline Tilings. *Phys. Solid State* **2015**, *57*, 810–814. [CrossRef]
8. Jungck, J.R.; Brittain, S.; Plante, D.; Yarbrough, J.; Zeller, C. Self-Foldability of Dürer Net Models of Viral Capsids: Exploring Nanocapsule Design via 4D Printing. *Math. Model. Nat. Phenom.* 2025, *in press*. [CrossRef]
9. Dodd, P.M.; Damasceno, P.F.; Glotzer, S.C. Universal Folding Pathways of Polyhedron Nets. *Proc. Natl. Acad. Sci. USA* **2018**, *115*, 6690–6696. [CrossRef]
10. Kaplan, C.S. *Introductory Tiling Theory for Computer Graphics*; CRC Press: Boca Raton, FL, USA, 2021.
11. Khiripet, N.; Khantuwan, W.; Jungck, J.R. Ka-me: A Voronoi Image Analyzer. *Bioinformatics* **2012**, *28*, 1802–1804. [CrossRef]
12. Jungck, J.R.; Pelsmajer, M.J.; Chappel, C.; Taylor, D. Space: The Re-Visioning Frontier of Biological Image Analysis with Graph Theory, Computational Geometry, and Spatial Statistics. *Mathematics* **2021**, *9*, 2726. [CrossRef]
13. Li, H. Generalizations of Dirac's Theorem in Hamiltonian Graph Theory—A Survey. *Discret. Math.* **2013**, *313*, 2034–2053. [CrossRef]
14. Dirac, G.A. Some Theorems on Abstract Graphs. *Proc. Lond. Math. Soc.* **1952**, *s3-2*, 69–81. [CrossRef]
15. Ore, O. Note on Hamilton Circuits. *Am. Math. Mon.* **1960**, *67*, 55. [CrossRef]
16. Esque, J.; Oguey, C.; de Brevern, A.G. Comparative Analysis of Threshold and Tessellation Methods for Determining Protein Contacts. *J. Chem. Inf. Model.* **2011**, *51*, 493–507. [CrossRef]
17. Gardner, M. Extraordinary Nonperiodic Tiling That Enriches the Theory of Tiles. *Sci. Am.* **1977**, *236*, 110–121. [CrossRef]
18. Gardner, M. *Penrose Tiles to Trapdoor Ciphers: And the Return of Dr Matrix*; Cambridge University Press: Cambridge, UK, 1997.
19. de Bruijn, N.G. Algebraic Theory of Penrose's Non-Periodic Tilings of the Plane I, II. *Indag. Math.* **1981**, *84*, 39–66. [CrossRef]
20. Doroba, A.; Sokalski, K. The Time-Dependent Ising Model on the 2D Penrose Lattice. *Phys. Status Solidi (b)* **1991**, *167*, 251–264. [CrossRef]
21. Gummelt, P. Penrose Tilings as Coverings of Congruent Decagons. *Geom. Dedicata* **1996**, *62*, 1–17. [CrossRef]
22. Flicker, F.; Simon, S.H.; Parameswaran, S.A. Classical Dimers on Penrose Tilings. *Phys. Rev. X* **2020**, *10*, 011005. [CrossRef]
23. Ghose, A. Hands-On Exploration of Tessellation and Fractal Mapping on a Tiling Wall to Enhance Interest in Doing Maths in Non-Formal Settings. *J. Sci. Temper* **2021**, *9*, 33–60.
24. Yan, X.; Yan, W.Q.; Liu, L.; Lu, Y. Penrose Tiling for Visual Secret Sharing. *Multimed. Tools Appl.* **2020**, *79*, 32693–32710. [CrossRef]
25. Caspar, D.L.D.; Klug, A. Physical Principles in the Construction of Regular Viruses. *Cold Spring Harb. Symp. Quant. Biol.* **1962**, *27*, 1–24. [CrossRef]
26. Dye, D. *The New Book of Chinese Lattice Designs*; Dover Publications: New York, NY, USA, 1981.
27. Sloane, N.J.A. Deltoidal Trihexagonal Tiling. In *The On-Line Encyclopedia of Integer Sequences (OEIS)*; The OEIS Foundation Inc.: Highland Park, NJ, USA, 2020. Available online: https://oeis.org/A272463 (accessed on 10 September 2025).
28. Boggs, G. Of Hexagons, Kites, and Tiles. *Ology Blog*. 30 April 2023. Available online: https://ology.github.io/2023/04/30/of-hexagons-kites-and-tiles/ (accessed on 10 September 2025).
29. Coulbois, T.; Gajardo, A.; Guillon, P.; Lutfalla, V. Aperiodic Monotiles: From Geometry to Groups. *arXiv* **2024**, arXiv:2409.15880. [CrossRef]
30. Shutov, A.V.; Maleev, A.V. Penrose Tilings as Model Sets. *Crystallogr. Rep.* **2015**, *60*, 797–804. [CrossRef]
31. Shutov, A.V.; Maleev, A.V. Coordination Numbers of the Vertex Graph of a Penrose Tiling. *Acta Crystallogr. Sect. A* **2018**, *74*, 112–122. [CrossRef]
32. Williams, J. Geometry and Art. In *Multicultural Mathematics: Teaching Mathematics from a Global Perspective*; Nelson, D., Joseph, G.G., Williams, J., Eds.; Oxford University Press: Oxford, UK, 1993; pp. 142–174.
33. Ouazene, Z. Quasi-Periodic Tiling in Moroccan and Andalusian Decorative Art: A Harmonious Symphony of Mathematics and Aesthetics. In Proceedings of the 5th International Conference on Advanced Technologies for Humanity (ICATH'2023), Rabat, Morocco, 25–26 December 2023; Springer: Cham, Switzerland, 2023; pp. 22–37.
34. Cromwell, P.R. Cognitive Bias and Claims of Quasiperiodicity in Traditional Islamic Patterns. *Math. Intell.* **2015**, *37*, 30–44. [CrossRef]
35. Kerins, B.; Yong, D.; Cuoco, A.; Stevens, G.; Pilgrim, M. *Fractions, Tilings, and Geometry*; American Mathematical Society: Providence, RI, USA, 2018.
36. Blumeyer, D. Aperiodic Monotiles. *Sagittal Forum*. 2023. Available online: https://forum.sagittal.org/viewtopic.php?t=569 (accessed on 10 September 2025).
37. Grünbaum, B.; Shephard, G.C. *Tilings and Patterns*; W.H. Freeman and Company: New York, NY, USA, 1987.
38. Le, T.T.Q. Local Rules for Quasiperiodic Tilings. In *The Mathematics of Long-Range Aperiodic Order*; Moody, R.V., Ed.; NATO ASI Series C: Mathematical and Physical Sciences; Kluwer Academic Publishers: Dordrecht, The Netherlands, 1997; Volume 489, pp. 331–366.
39. Voigt, J.; Baljozović, M.; Martin, K.; Wäckerlin, C.; Avarvari, N.; Ernst, K.H. An Aperiodic Chiral Tiling by Topological Molecular Self-Assembly. *Nat. Commun.* **2025**, *16*, 83. [CrossRef]

40. Adams, C. *The Tiling Book: An Introduction to the Mathematical Theory of Tilings*; American Mathematical Society: Providence, RI, USA, 2022.
41. Friedman, E. Heesch Tiles with Surround Numbers. Available online: https://erich-friedman.github.io/papers/heesch/heesch (accessed on 10 September 2025).
42. Mann, C. Heesch's Tiling Problem. *Am. Math. Mon.* **2004**, *111*, 509–517. [CrossRef]
43. Weisstein, E.W. Heesch Number. MathWorld—A Wolfram Web Resource. Available online: https://mathworld.wolfram.com/HeeschNumber.html (accessed on 10 September 2025).
44. Locke Demosthenes. Aperiodic Monotile with Hole in It. Math StackExchange. 2023. Available online: https://math.stackexchange.com/q/4674746 (accessed on 10 September 2025).
45. Kaplan, C.S. Heesch Numbers, Part 1. *Isohedral Blog*. 2017. Available online: https://isohedral.ca/heesch-numbers-part-1/ (accessed on 10 September 2025).
46. Phillips, D. Tessellation. *Wiley Interdiscip. Rev. Comput. Stat.* **2014**, *6*, 202–209. [CrossRef]
47. Goucher, A.P. Aperiodic Monotile. *cp4space Blog*. 21 March 2023. Available online: https://cp4space.hatsya.com/2023/03/21/aperiodic-monotile (accessed on 10 September 2025).
48. Gilevich, A.; Shoval, S.; Nosonovsky, M.; Frenkel, M.; Bormashenko, E. Converting Tessellations into Graphs: From Voronoi Tessellations to Complete Graphs. *Mathematics* **2024**, *12*, 2426. [CrossRef]
49. Wheatley, J.-P. The Hat Trick: A 3D-Printed Polyhedron of Hat Tiles. Available online: https://jonpaul.com (accessed on 10 September 2025).
50. Akpanya, R.; Goertzen, T.; Liu, Y.; Stüttgen, S.; Robertz, D.; Xie, Y.M.; Niemeyer, A.C. Constructing Topological Interlocking Assemblies Based on an Aperiodic Monotile. In Proceedings of the IASS 2024 Symposium: Redefining the Art of Structural Design, Zurich, Switzerland, 26–30 August 2024; IASS: Zurich, Switzerland, 2024; pp. 26–30.

Disclaimer/Publisher's Note: The statements, opinions and data contained in all publications are solely those of the individual author(s) and contributor(s) and not of MDPI and/or the editor(s). MDPI and/or the editor(s) disclaim responsibility for any injury to people or property resulting from any ideas, methods, instructions or products referred to in the content.